ELSEVIER

Contents lists available at ScienceDirect

# Advances in Water Resources

journal homepage: www.elsevier.com/locate/advwatres





# Evolution of pore-scale concentration PDFs and estimation of transverse dispersion from numerical porous media column experiments

Saif Farhat a,\*, Guillem Sole-Mari b, Daniel Hallack a, Diogo Bolster a

- <sup>a</sup> University of Notre Dame, Notre Dame, 46556, IN, United States of America
- <sup>b</sup> University of Rennes, Rennes, 35065, Bretagne, France

#### ARTICLE INFO

Dataset link: https://zenodo.org/records/1044 2631

Keywords:
Pore-scale concentrations
Mixing
Probability density function
Boundary effects
Computational Fluid Dynamics

### ABSTRACT

Knowing local concentration distributions is important for transport and mixing, particularly in porous media, yet a comprehensive understanding of them remains a challenge. Computing advancements have enabled highresolution pore-scale simulations, offering an unprecedented opportunity for in-depth investigation of mixing. In this study we use simulation data to examine concentration distributions at the pore scale in the context of longitudinal (pseudo-one-dimensional) solute transport through a porous column. These distributions arise in a single column from heterogeneous flow at the pore-scale, which gets averaged out when upscaled and are not with reference to statistics across multiple random realizations. To measure these distributions, we first devise a semi-analytical approach to estimate the mean effective transport velocity profile for a non-uniform Darcy-scale fluid velocity, which unavoidably occurs due to the presence of lateral boundaries. This development allows sampling micro-scale concentrations over a moving surface that possesses a well defined Darcy-scale mean concentration, enabling empirical computation of the local concentration distribution. As an added benefit we find that our approach allows for the estimation of transverse dispersion coefficients, which is not typical in traditional column experiments. The implemented approach can estimate it via inverse modeling, and it agrees closely with previously published experimental data across the range of Peclet numbers we studied. We found that the measured pore-scale concentration probability density functions are best represented by a beta distribution, thus validating this longstanding hypothesis with direct evidence. Furthermore, we propose a model to describe the temporal and spatial evolution of the local concentration pdf, as well as its Péclet number dependence.

## 1. Introduction

Prediction of the environmental ramifications of groundwater contamination should include knowledge of the spatial extent of a plume, its temporal evolution, and prediction of the range of potential concentrations. Detailed knowledge of the distribution of concentrations is particularly important when trying to understand mixing processes and possible chemical reactions, which are typically nonlinear in nature. Using the classical Advection-Dispersion equation is not always, if ever, reliable. This is because of the presence of heterogeneity and incomplete mixing at all scales that is not adequately accounted for (Kapoor et al., 1997; Gramling et al., 2002; Tartakovsky et al., 2009), which can lead to a noticeable overestimation of reaction rates as demonstrated by experiments (Raje and Kapoor, 2000; Gramling et al., 2002; Anna et al., 2014) and numerical studies (Rubio et al., 2008; Liu and Mostaghimi, 2018; Sole-Mari et al., 2022). Yet, the accurate prediction of reactive transport is important across diverse applications, including

contaminant transport, geological carbon sequestration, and nuclear waste disposal to name a few (Liu and Mostaghimi, 2018; Valocchi et al., 2019).

Recent high performance computing, high-resolution pore-scale simulations that are capable of capturing the details of this incomplete mixing behavior offer an unprecedented opportunity to investigate such phenomena in depth. In particular, the simulations presented in Sole-Mari et al. (2022) recreate a minimal representative porous media column experiment. They used high performance computing to simulate conservative transport in a column with high spatial and temporal resolution. While previous studies have simulated incomplete mixing and reactions at pore scales (Bijeljic et al., 2013; Alhashmi et al., 2015; Liu and Mostaghimi, 2018), they were performed on relatively small domains with a dimension of a few millimeters that might not be enough to allow for the complete evolution of mixing dynamics.

E-mail address: sfarhat@nd.edu (S. Farhat).

Corresponding author.

The Sole-Mari et al. (2022) simulations are, to our knowledge, the first to attain a scale representative of a column experiment.

Multiple studies have developed mathematical models for the evolution of spatio-temporal fluctuations of local-scale concentrations under both conservative and reactive transport in porous media (Bellin and Tonina, 2007; Dentz and Tartakovsky, 2010; Bellin et al., 2011). For the sake of parsimony, as well as relevance for many systems of interest, a commonly studied reactive transport scenario is the limiting case where reactions are instantaneous and irreversible, and all reacting species have an identical seepage velocity and diffusion coefficient. The reason for this is that the full details of the reactive scenario can be predicted from purely conservative transport data. Thus, if we can accurately predict fluctuations in conservative transport concentrations, it also enables us to comprehend them in a reactive setting.

An increasingly successful but to date unsubstantiated modeling approach is to represent concentration variability within a representative elementary volume as a probability density function assuming a beta distribution. The advantage of this distribution is that it is a highly flexible bounded function with only two shape parameters. Oates and Harvey (2007) proposed partial-differential equations for the evolution of the mean and variance of concentrations and calibrated the beta distribution parameters to fit experimental reactive data in a heterogeneous porous medium. Chiogna and Bellin (2013) derived an analytical expression of the beta pdf variance decay over time to describe reactive transport in porous media. One drawback of their approach is the necessity to calibrate their model parameters using an existing concentration profile. In their study, they used the data of Gramling et al. (2002) and successfully applied their model to it. However, while their model successfully predicted observed mean behaviors, the underlying assumption of a beta distribution was not explicitly tested and validated.

To understand incomplete mixing, it is beneficial to investigate the mixing interface where physical contact between reactive species takes place. This interface is distorted by the velocity field in heterogeneous systems. Several theoretical approaches exist to explore this. For example, there exists (i) volume averaging (Bolster et al., 2011) that can approximate the concentration distribution of a conservative species in order to quantify nonlinear mixing effects; (ii) estimating the effective dispersion coefficient of the Green's function to account for the role of transverse diffusion, which can be used to predict mixing quite accurately (Perez et al., 2019); (iii) a lamellar depiction of mixing, where a scalar mixture can be viewed as a collection of lamellae undergoing changes through stretching, diffusion, and coalescence (Le Borgne et al., 2015) and (iv) a dual-scale framework (coarse and local), where the concentrations at local scale undergo a process of relaxation as they gradually converge towards the concentration values observed at the coarse scale (e.g. Multi Rate Interaction by Exchange with the Mean (MRIEM) model (Sole-Mari et al., 2020)).

While Darcy-scale heterogeneities arise in many experimental and natural settings, it is also important to note that the presence of boundaries can have a non-trivial influence on the flow and transport in any laboratory experiment or numerical simulation. A typical example in laboratory experiments involving granular materials is the significant (and often undesired) alteration of grain arrangement, permeability, and fluid velocity near the lateral walls. In a numerical setting, boundary effects can be reduced by imposing a fully periodic boundary condition (Bazarin et al., 2021). While it may solve the boundary problem, some might argue it compromises a true description of reality in other ways. However, our main point is that boundary effects remains often undiscussed issue in both simulations and experiments even when preventative measures are taken. In this paper, to tackle this, we propose a semi-analytical approach for approximating the average effective transport velocity profile in the presence of non-uniform fluid velocity at the Darcy scale. We apply this approach to the simulations of Sole-Mari et al. (2022) to extract the local concentration variability along the mixing interface. Then, we apply Maximum Likelihood Estimation

(MLE) to test if the beta pdf is indeed the most adequate representation of the local concentration distributions. Finally, we provide a mathematical description to estimate the change in the variance of the local concentration distribution with time and space.

#### 2. Simulation

Many numerical simulations of flow and transport in porous media found in the literature are either two dimensional (Acharya et al., 2007; Rolle et al., 2013), thus limiting the degrees of freedom relative to real settings, or, due to computational costs, three-dimensional with small domain sizes (Bijeljic et al., 2013; Alhashmi et al., 2015; Liu and Mostaghimi, 2018) thus not capturing the full development of mixing fronts over sufficient time to attain asymptotic behavior. In this paper, we used the pre-existing pore-scale simulations from Sole-Mari et al. (2022) to conduct our analysis. In this section we provide a brief overview of this simulation set, but for full details we direct the reader to Sole-Mari et al. (2022).

#### 2.1. Characteristics of the column simulation

To create a random porous medium that resembles a column such as the one in the experiment of Gramling et al. (2002), spherical solid grains with a uniform diameter  $d_0$  were allowed to settle by gravity into an empty column using *Blender*. This is an open-source 3D computer graphics and animation software with rigid body physics simulation capabilities. Then an outer portion of the domain was cut off and discarded in order to get rid of boundary effects on the packing geometry and properties.

The simulations were conducted using various utilities of the open-source Computational Fluid Dynamics (CFD) software OpenFOAM. A cubic regular mesh with a cell size of  $d_0/60$  was transformed into an unstructured mesh using the  $\it snappyHexMesh$  utility to accurately capture the grain-fluid interface. Fig. 1 shows the full column dimensions, a detailed sample portion of it and the finite volume mesh. This unstructured mesh was used to solve the steady-state, incompressible Navier–Stokes equations

$$(\boldsymbol{u} \cdot \nabla)\boldsymbol{u} = \nu \nabla^2 \boldsymbol{u} - \frac{1}{\rho} \nabla p \,, \tag{1}$$

where the velocity field is denoted by  $\boldsymbol{u}$   $(LT^{-1})$ , kinematic viscosity by v  $(L^2T^{-1})$ , and the pressure gradient by  $\nabla p$   $(L^2T^{-2})$ . No-slip boundary conditions are enforced at the fluid-grain interface. Meanwhile, a full-slip boundary condition was applied to the column's transverse boundaries. This condition enforces a zero-shear stress at the side walls, aiming to minimize their influence within the bounded domain on flow and transport dynamics.

Even though the Reynolds number was about 0.2, which would fall into the Stokes flow regime where inertial forces are much smaller than the viscous forces  $[(\boldsymbol{u}\cdot\nabla)\boldsymbol{u}\ll v\nabla^2\boldsymbol{u}]$ , the advective inertial term was still solved for in the simulation.

# 2.2. Conservative and reactive transport

After the flow field has been solved at the pore scale, the advectiondiffusion equation was used to simulate the transport of a conservative scalar. This reads

$$\frac{\partial C}{\partial t} = -\mathbf{u} \cdot \nabla C + D\nabla^2 C,\tag{2}$$

where the concentration is denoted by C ( $ML^{-3}$ ), and the diffusion coefficient by D ( $L^2T^{-1}$ ).

The inlet boundary condition is a continuous injection with a Heaviside step function initial condition located a distance of 4.5  $d_0$  from the inlet. Meanwhile, the outlet boundary condition is a Neumann boundary condition with zero-gradient, with side walls enforcing no-flux

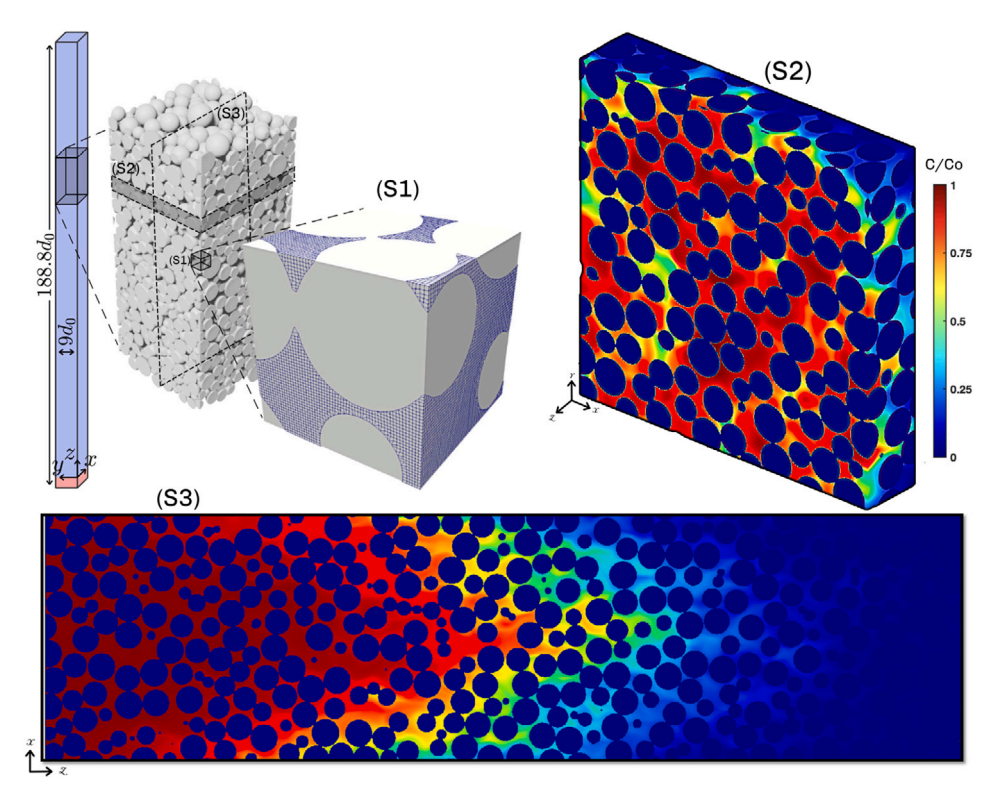


Fig. 1. Full simulation column dimensions  $(9d_0, 9d_0, 188.8d_0)$  and an example portion of it (S1) Finite volume unstructured mesh that was used in the simulation (S2) Slice cut of the domain at the mixing interface for conservative transport (S3) Longitudinal cross section of normalized concentrations for conservative transport.

conditions. Sections 2 and 3 (S2 and S3) in Fig. 1 depict sample cross-sectional and longitudinal views of the moving interface of normalized concentrations for conservative transport. Six grain Péclet number cases with  $Pe=10,\ 32,\ 100,\ 316,\ 1000,\ and\ 3160$  were simulated by changing the molecular diffusion coefficient, where the grain Péclet number is defined as:

$$Pe = ud_0/D. (3)$$

This range of Péclet numbers encompasses regimes where diffusion significantly influences transport, transitioning to regimes where advection dominates.

Conservative transport can be reinterpreted to understand reactive transport. First, define two reactants A (invading) and B (resident), whose product is C. By assuming an instantaneous irreversible reaction, one can define two reaction independent, conservative species  $u_A$  and  $u_B$ , as:

$$u_A = C_A + C_C \,, \tag{4}$$

$$u_B = C_B + C_C \,. \tag{5}$$

By simulating conservative transport, the reactive counterpart can be evaluated by stating that due to the instantaneous nature of the reaction A and B cannot coexist at the same point in space and time; thus the concentration of product C can be calculated as:

$$C_c(z,t) = \min(u_A(z,t), u_B(z,t)). \tag{6}$$

This will be used to quantify the reaction product C, highlighting any incomplete mixing. Additionally, in this context, the 0.5 isoconcentration line from the conservative transport simulations is analogous to the mixing interface between the reactants. Therefore, we will use these terms interchangeably throughout the paper.

### 3. Semi-analytical approach to track mixing interface deformation

We aim to investigate the spatial and temporal evolution of the local probability density function (pdf) of concentrations under upscaling to Darcy-scale-uniform flow and transport. At that scale, our column is modeled as one-dimensional, provided that the flow really is uniform aside from the random fluctuations exerted by pore-scale features. Under such conditions, one could examine for instance the thin transverse slice of medium over which the mean concentration at a given time is  $\bar{c}=0.5$ , and compute the local concentration distribution around that mean value, which characterizes pore-scale concentration fluctuations.

Unfortunately, the condition of a uniform Darcy flow is extremely difficult to fully achieve in a bounded medium such as our column, where the typical flow profile over a cross-section exhibits some boundary effect. Despite the efforts implemented towards minimizing it by (i) ensuring stationary statistics for the grain packing and (ii) imposing a full-slip boundary condition at the lateral walls (see Sole-Mari et al. (2022)). Here, we clarify that the boundary effect we note arises from the presence of the lateral walls themselves. Despite having a full-slip boundary conditions, grains intersecting the boundary still exert a no-slip boundary condition and the imposition of no flow across the boundaries, leads to an average slowdown near the lateral walls, as shown by the longitudinally averaged velocity profile in Fig. 2(b). Consequently, the mixing interface in the transport simulations has a tendency to become curved (faster in the center than in the corners) as time advances (see Fig. 1 (S3)).

The concentration distribution over a flat slice of medium, as in Fig. 1 (S2), will therefore contain information about both the boundary effect and the pore-scale fluctuations, which is difficult to disentangle. To prevent this, we aim to replace the flat-slice sampling, which is based on the assumption of a uniform Darcy-scale flow, with a curved slice that deforms following the apparent Darcy-scale velocity profile of the mixing interface. In order to do this, we first need to conceptually separate the scales. We distinguish the Darcy-scale velocity profile (which includes the boundary effect but is otherwise smooth) from the pore-scale velocity fluctuations by noting that the former would emerge from averaging the flow field over a large number of random realizations of the grain packing, whereas the latter would be washed out by this averaging. Since such data from multiple realizations are

not available, we use the longitudinally averaged velocity profile as a proxy for the Darcy-scale velocity profile. Then, in order to derive the apparent velocity profile of the mixing interface, we model Darcy-scale transport as (i) longitudinal advection and (ii) transverse dispersion. The latter is an adjustable parameter. We ignore longitudinal dispersion, focusing solely on local transverse dispersion as the process responsible for exchanging solute mass between different streamlines (Oya and Valocchi, 1998; Cirpka and Kitanidis, 2001).

Our approach is conceptually similar to contaminant source identification methods described in the literature (e.g. Wilson and Liu (1994) and Liu and Wilson (1995)). They solved the transport equation using stochastic differential equations backwards in time, keeping the dispersion part positive while reversing advection. However, unlike the usual focus on longitudinal positions in the literature (Atmadja and Bagtzoglou, 2001), we aim to estimate the expected transverse position. We first note the relationship between the Darcy-scale transport solution for a Heaviside step function and the one for a Dirac delta function: the latter is the longitudinal spatial derivative of the former. A helpful analogy is to view the continuous injection; with Heaviside step function initial condition; as a cumulative density function (cdf) and the pulse injection result as its pdf. As such, the  $\bar{c}=0.5$  isosurface for the former will correspond to the median longitudinal position of the latter.

Let us consider the concentration field using a particle representation. Then, using the mean position as an approximation for the median position, we can thus assume that the Darcy-scale mixing interface longitudinal position  $z_{iif}(t;x,y)$  is given by the expected value of z among all solute particles with transverse position  $x_t, y_t$  at time t, with all particles originating from a Dirac delta function initial condition.

The expected *z*-position of a particle which lies on  $x_t, y_t$  at time *t* can be derived from its expected history of velocities, which, under the assumption of a longitudinal Darcy-scale velocity profile that is constant in *z*, is a direct consequence of the probabilistic and temporal distribution of x, y positions. Neglecting for now the domain's bounds, the position history distribution  $P(x, y, t)|_{x_t, y_t}$  can be obtained by integrating the Green's function (Polyanin, 2001) for diffusion over time and assuming a Fickian transverse dispersion as:

$$P(x, y, t)|_{x_t, y_t} = \frac{1}{t} \int_0^t \frac{1}{4\pi \sqrt{D_x D_y}(t-\tau)} \exp\left(\frac{-(x-x_t)^2}{4D_x(t-\tau)} + \frac{-(y-y_t)^2}{4D_y(t-\tau)}\right) \partial \tau.$$
 (7)

The normalization by t ensures that the spatial integral of P(x,y,t) is 1, making it a proper probability density estimate. Here we denote two different transverse dispersion coefficients  $(D_x,D_y)$  so the solution is generalized to anisotropic cases. By solving the integral in Eq. (7) by substitution and recalling the definition of the exponential integral  $E_1(\xi)$ ,

$$E_1(\xi) = \int_{\xi}^{\infty} \frac{1}{t} \cdot e^t \partial t \,. \tag{8}$$

We get the unbounded solution of (7) as:

$$P(x,y,t)|_{x_t,y_t} = \frac{1}{4\pi\sqrt{D_xD_y}t}E_1\left(\frac{(x-x_t)^2}{4D_xt} + \frac{(y-y_t)^2}{4D_yt}\right) \ . \tag{9}$$

The boundary condition at the external walls (no diffusive flux) can be implemented via reflection of the Green's function (Szymczak and Ladd, 2003). To emulate reflection, a number 2n of virtual sources can be placed outside the domain  $x \in [-k, k]$  and  $y \in [-h, h]$ , where h and k are the distances from the domain center to the x and y boundaries respectively:

$$P(x,y,t)|_{x_t,y_t} = \sum_{i=-n}^{n} \sum_{j=-n}^{n} \frac{1}{4\pi\sqrt{D_x D_y t}} E_1\left(\frac{(x-x_t-2ik)^2}{4D_x t} + \frac{(y-y_t-2jh)^2}{4D_y t}\right),$$
(10)

where, theoretically,  $n \to \infty$ . In practice, n is sufficiently large so that the volume under surface (10) within  $x \in [-k, k]$  and  $y \in [-h, h]$  is

equal to the total volume under the unbounded surface (9). Eq. (10) is the general solution for the bounded (x,y) position history distribution for any particle found on  $(x_t,y_t)$  at time t. At time  $t \to 0$  the particle position history takes the shape of a Dirac delta  $\delta(x-x_t,y-y_t)$ , assigning probability one to the singular position  $(x_t,y_t)$ . Hence, in this case the particle carries the velocity  $u_o(x_t,y_t)$ . At time t>0, the warped surface velocity, for any given transverse position  $x_t,y_t$ , can be calculated via convolution of (I)  $P(x,y,t)|_{x_t,y_t}$  (Eq. (10)) and (II) the mean longitudinal velocity  $u_0(x,y)$  (Fig. 2(b)) as:

$$u_{warped}(t)|_{x_{t},y_{t}} = \iint_{\Omega} P(x,y,t)|_{x_{t},y_{t}} u_{o}(x,y) \partial x \partial y \simeq \frac{\sum (P(x,y,t)|_{x_{t},y_{t}} u_{o}(x,y))}{\sum P(x,y,t)|_{x_{t},y_{t}}}.$$
(11)

To get the velocity of the entire warped surface, simply apply the previous approach to a raster that covers the domain width  $\Omega$  (in our case  $x_t \in [0\ 9d_0]$ ,  $y_t \in [0\ 9d_0]$ ). We found a raster resolution of approximately 0.25 to 0.5 grain radii to be sufficient. For large t (i.e.,  $t\gg \max(k^2/D_x,h^2/D_y)$ ),  $P(x,y,t)|_{x_t,y_t}$  approaches a uniform distribution with a  $\frac{1}{4kh}$  probability. Thus, the time-averaged longitudinal velocity at any  $(x,y,t,x_t,y_t)$  can be approximated by the global spatial mean velocity  $\bar{u}$ . This implies that the rate of longitudinal separation between any two random points  $(x_{t1},y_{t1})$ ,  $(x_{t2},y_{t2})$  goes to zero, suggesting that the deformation of the interface will eventually stagnate.

The same approach can also be used for a two-dimensional domain, that is a one-dimensional cross-section. In this case, the transverse position history distribution  $P(y,t)|_{y_t}$  (assuming a mean flow along the x axis) would be:

$$P(y,t)|_{y_t} = \sum_{n=-\infty}^{\infty} \frac{|y - y_t - 2nh|}{4\sqrt{\pi}D_y t} \Gamma\left[-0.5, \frac{(y - y_t - 2nh)^2}{4D_y t}\right],$$
 (12)

where  $\Gamma[\eta, z]$  is the upper incomplete gamma function, defined as:

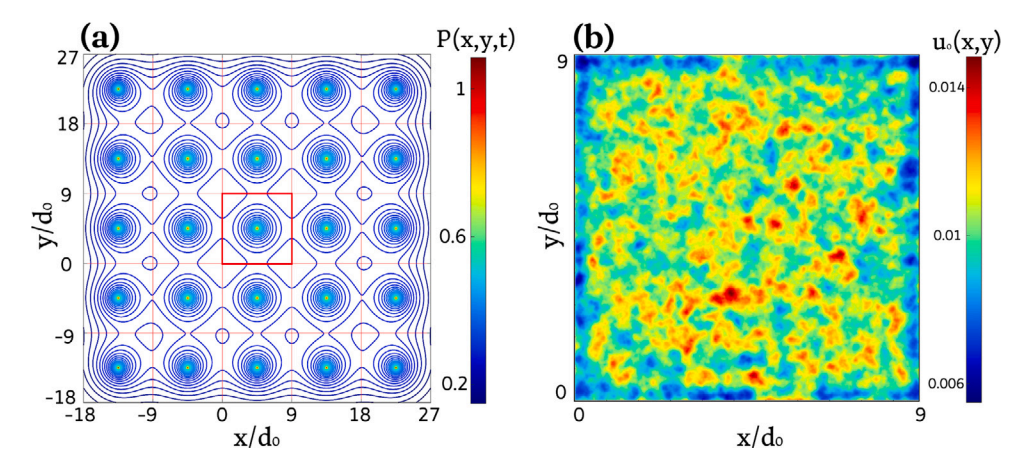
$$\Gamma[\eta, z] = \int_{z}^{\infty} t^{\eta - 1} e^{-t} \partial t.$$
 (13)

Fig. 2(a) depicts  $P(x,y,t)|_{x_t,y_t}$  (i.e., the solution of Eq. (10)) as a contour plot, for  $(x_t,y_t)=(0,0)$  and n=2, with arbitrary values of  $D_x=D_y$  and at an arbitrary time t. Fig. 2(b) shows a heatmap of the mean longitudinal velocity  $u_o(x,y)$ . Convolution between these two functions returns the time-averaged particle velocity at  $(x_t,y_t)$  and time t, which, as explained above, closely corresponds to the apparent velocity of the  $\bar{c}=0.5$  iso-concentration surface.

The value of the transverse dispersion coefficients  $D_x$ ,  $D_y$  is unknown *a priori*. Since the medium's geometry is fully isotropic, we can assume  $D_x = D_y = D_T$ . Then the value of  $D_T$  can be determined by inverse modeling, in our case by finding the value that minimizes the root mean square deviation between the semi-analytical solution and the actual iso-concentration surface from the simulation data.

An unintended, yet powerful, consequence of this approach is that we can exploit the inadvertent influence of the boundaries to get the added benefit of estimating transverse dispersion from "one-dimensional" column data by accounting for measurable transverse effects. We note that this approach is not limited to this specific mean-longitudinal velocity profile; it is equally suitable for any other non-uniform Darcy-scale velocity profiles. As a check for our method we compare out estimates of transverse dispersion to published values. In a comprehensive study, Delgado (2007) consolidated transverse dispersion measurements from 15 different papers and experiments. Over the range of Péclet numbers simulated, our measurements of transverse dispersion coefficients, represented by the red circles in Fig. 3, align closely with the available data..

Fig. 4 offers an illustrative direct comparison between the concentration distribution sampled by a transverse plane that moves at the mean longitudinal velocity versus the corresponding distribution sampled by a warped surface that accounts for the boundary effect as



**Fig. 2.** Implementation of the semi-analytical solution to calculate the mixing interface deformation, (a) Sample solution of Eq. (10) for a point at the center of the domain  $(x_i, y_i)$  at an arbitrary time with the virtual sources field. (b) Collapsed velocity profile in the *z*-direction of the simulation.

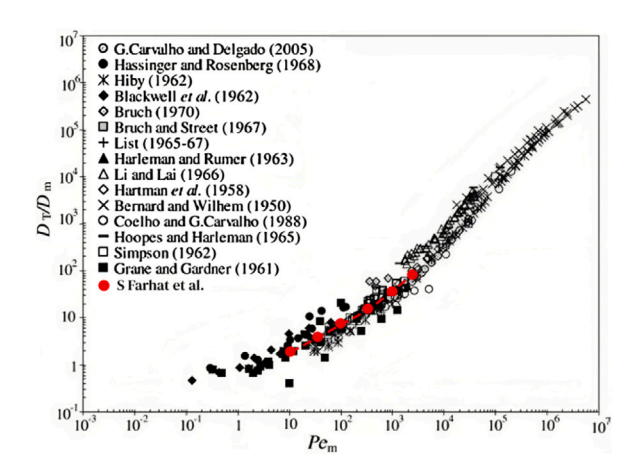


Fig. 3. Transverse dispersion  $(D_T/D_m)$  versus  $Pe_m$  quantified using semi-analytical solution compared to data from Delgado (2007).

detailed here. The former results, as shown in Fig. 4(a), are clearly influenced by a mean inward concentration gradient, leading to a probability density function estimate that does not accurately represent pore-scale incomplete mixing in a one-dimensional uniform velocity interpretation. Both an overestimation of the variance and artificial skewness are observed in the distribution. On the other hand, usage of the warped sampling surface (figure 4(b)) is able to decouple the pore-scale incomplete mixing from the boundary distortion. In this case, the pdf is much more symmetric and has lower variance. A more thorough investigation is carried out in the next section in order to robustly identify the form of pdf that best represents these concentration distributions.

Lastly, we note that the incomplete mixing reported in the literature (Raje and Kapoor, 2000; Gramling et al., 2002; Chiogna and Bellin, 2013; Sole-Mari et al., 2022) is likely often overestimated. To assess this, we compare the one-dimensional reaction product concentration  $C_c$ , as quantified by the Standard Pore-Scale Mixed (SPSM) model using Eq. (6) (Gramling et al., 2002) to the observed concentrations both with and without considering the boundary effect. The SPSM model assumes that concentrations are effectively "well mixed" at the pore scale. When the wall effects are relaxed using the approach outlined in this section, one observes that the one-dimensional reaction product concentration aligns more closely with the well-mixed estimation, as shown in Fig. 4(c). We still observe incomplete mixing, but just less of it.

### 4. Probability density function

Due to the heterogeneous nature of velocity fields in porous media which leads to mixing-limited reactions, quick and reliable predictions of reactive transport are often unavailable. While simulations like those of Sole-Mari et al. (2022), where flow and transport are fully resolved at the pore scale, are great test cases to explore reactive transport in porous media, computational costs render them impractical for common applications. Here we use these simulations to develop and test an upscaled stochastic model based on the concentration probability density function that captures the effect of heterogeneity and incomplete mixing.

We use the semi-analytical approach described in the previous section to determine the Darcy-scale geometry of the mixing interface, denoted as  $z_{itf}(t;x,y)|_{\bar{c}=0.5}$ , and with this we obtain the pore-scale conservative concentrations  $u_A$ . We sample concentrations within a small distance of  $\pm 0.25d_0$  from  $z_{itf}(t;x,y)|_{\bar{c}=0.5}$ .

Fig. 5 (left) shows the temporal evolution of the pore-scale concentration pdf at  $z_{itf}(t;x,y)|_{\bar{c}=0.5}$  for Pe=100. At early times, the pdf is spread out with two peaks at concentration values 0 and 1. As time increases, the distribution becomes unimodal and concentrated around the mean. We also note that there is a brief intermediate time in which the distribution becomes quasi-uniform as can be seen from its representation at  $2.5t^*$ .

We use Maximum Likelihood Estimation (MLE) to optimize parameters of a broad family of probability density functions to best match the observed distributions of  $u_A$  across the simulated Péclet number cases. We test 20 different bounded and unbounded continuous pdfs (the full list is reported in Fig. 5 (right)).

By optimizing the likelihood function across various times (namely 7 points in time comprising the different regimes) we demonstrate that among the 20 distributions, the beta distribution emerges as the most reliable and representative probability density function (see Fig. 5 (right)). The Kumaraswamy pdf is also an adequate representation, which is not surprising as it is closely related to the beta pdf. Although it has a simpler, closed-form probability density function, its mean and variance formulas are more complicated than those of the beta distribution. Additionally, the beta pdf presents less outliers, as shown in Fig. 5 (right). Lastly, the model we propose in Section 5, which is based on the beta pdf assumption, can be adapted to obtain Kumaraswamy shape parameters if needed. The truncated normal distribution becomes a reliable approximation for the distribution at late times . However, it is inadequate for earlier times, or when sampling mean Darcy-scale concentrations other than 0.5 ( $\bar{c} \neq 0.5$ ).

With this in mind, we proceed assuming that the pore-scale concentration fluctuations are best captured by the beta probability density

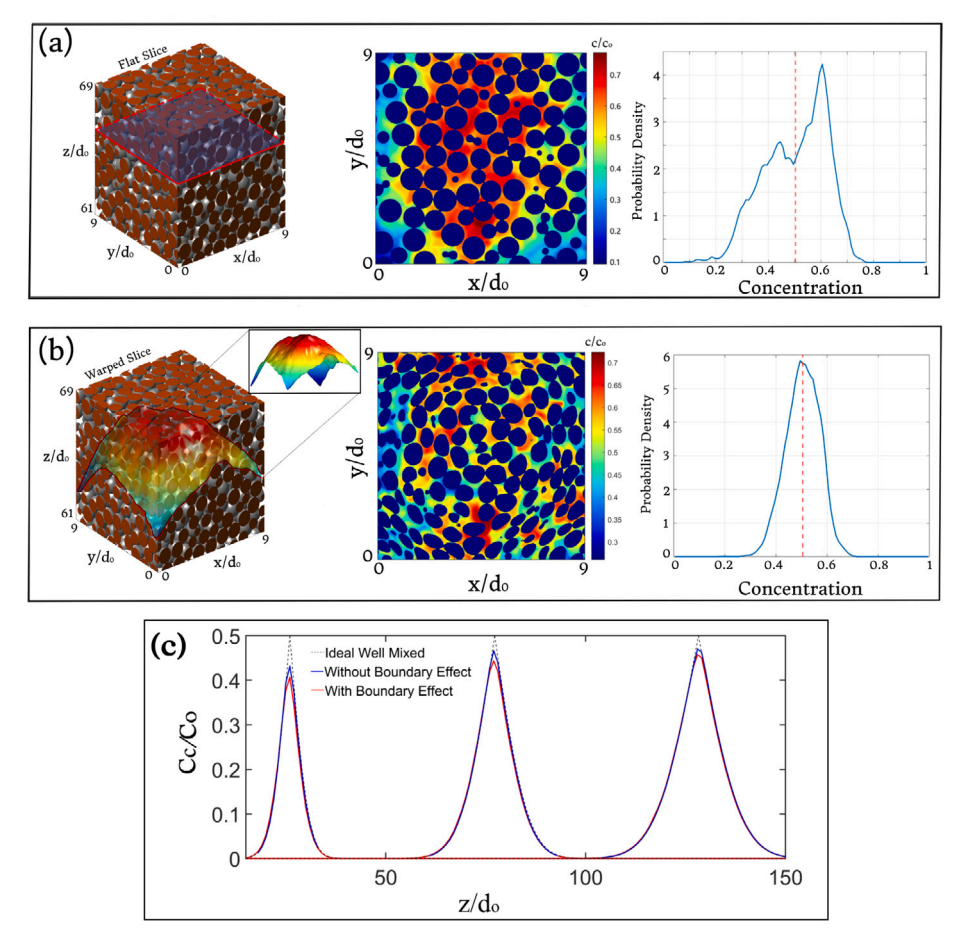


Fig. 4. Direct comparison between flat and warped sampling surfaces. (a) Sample cube of the domain with a flat slice located at the first moment showing the sampled concentrations distributions and probability density function (b) The same cube in (a) but illustrating the warped surface geometry and coordinates, it also shows the pore-scale concentration distribution and probability density function disentangled from the boundary effect (c) Measured one-dimensional reaction product concentration profiles at Peclet 10 with and without the boundary effect compared to the ideal well-mixed behavior at 25.7, 77.2, and 128.7 advection times.

function. It is supported on the interval [0 1] and is defined using two shape parameters  $\alpha$  and  $\beta$  (Elderton, 1906) as:

$$p_{\beta eta}(u_a) = \frac{u_a^{\alpha - 1} (1 - u_a)^{\beta - 1}}{B(\alpha, \beta)} , \tag{14}$$

where  $B(\alpha, \beta) = \Gamma(\alpha)\Gamma(\beta)/\Gamma(\alpha + \beta)$  and  $\Gamma$  is the Gamma function. The expected value and variance of the beta pdf are

$$E[u_a] = \frac{\alpha}{\alpha + \beta} \,, \tag{15}$$

$$Var(u_a) = \frac{\alpha\beta}{(\alpha+\beta)^2(\alpha+\beta+1)}.$$
 (16)

Fig. 6 shows the temporal evolution of the incomplete mixing concentration distributions at  $z_{iif}(t;x,y)|_{\tilde{e}=0.5}$  using a beta pdf. Conceptually, we divide it into two phases: an initial stage marked by double peaks at zero and maximum concentration that transitions later into a single peak, with a short-lived intermediate uniform structure. The signature of this two-phase behavior can be observed in the temporal decay of the variance of pore-scale concentrations as illustrated in Fig. 7(a). At the start of each simulation (t=0), regardless of the Péclet number, pdfs have a binary state of [0 1], thus the variance is 0.25. In purely advective systems ( $Pe = \infty$ ), this variance would not change, as illustrated by the dashed horizontal red line in Fig. 7(a), due to the lack of diffusion. However, in the presence of diffusion the variance decays from its maximum and eventually reaches a late time regime where  $\sigma^2 \propto t^{-1}$ . The transition to this was noted by Chiogna and Bellin (2013) as the time after which advection dominates over diffusion.

At the Darcy-scale mixing interface  $z_{itf}(t;x,y)|_{\tilde{\epsilon}=0.5}$ , due to symmetry, both distribution parameters  $\alpha$  and  $\beta$  should be equal. The

values obtained from fitting clearly validate that assumption aside from minor variations imputable to the diverse sources of uncertainty and randomness.. Thus we will henceforth assume that  $\alpha$  and  $\beta$  are always equal at  $z_{ilf}(t;x,y)|_{\bar{c}=0.5}$ . We do note, though, that they do differ when  $\bar{c} \neq 0.5$ , as we will explore in the following section.

# 5. Modeling spatial and temporal evolution of the beta pdf

To provide a mathematical description that accounts for incomplete mixing, we make a distinction between the mean of the beta pdf,  $\bar{c}$ , and the pore scale concentrations at  $z_{iif}(t;x,y)$ , represented as  $u_a$ . We assume that the former can be described by the 1-D solution of the advection–dispersion equation for a Heaviside initial condition at z=0 in an infinite domain (Ogata and Banks, 1961)

$$\bar{c}(z,t) = \frac{1}{2} \operatorname{erfc} \left[ \frac{z - ut}{\sqrt{4D_I t}} \right], \tag{17}$$

where z[L] is downstream distance,  $u[LT^{-1}]$  is the average pore velocity, and  $D_l[L^2T^{-1}]$  is the longitudinal dispersion coefficient. The porescale concentrations  $(u_a)$  follow the beta distribution as in Eq. (14), and their average is given by (17).

To avoid redundancy, let  $\eta=\alpha+\beta$ . With this, and using (15), Eqs. (14) and (16) are rewritten in terms of  $\eta$  and  $\bar{c}$  as

$$p_{\beta eta}(u_a) = \frac{u_a^{\bar{c}\eta} (1 - u_a)^{(1 - \bar{c})\eta}}{u_a (1 - u_a)} \cdot \frac{\Gamma[\eta]}{\Gamma[\bar{c}\eta] \Gamma[(1 - \bar{c})\eta]},$$
(18)

$$\sigma^2 = \frac{\bar{c}(1 - \bar{c})}{n + 1}.\tag{19}$$

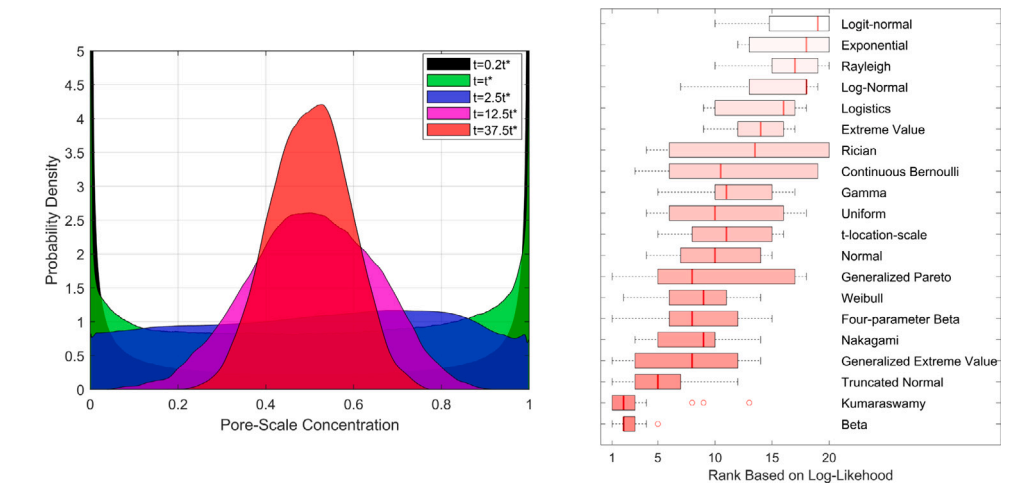


Fig. 5. (left) Concentrations pdfs at  $z_{iif}(t;x,y)|_{\tilde{c}=0.5}$  for Pe=100 at 0.2, 1, 2.5, 12.5, 37.5 advection times (t\*) (right) Ranking based on Log-Likelihood of 20 tested continuous distributions for the six Péclet numbers.

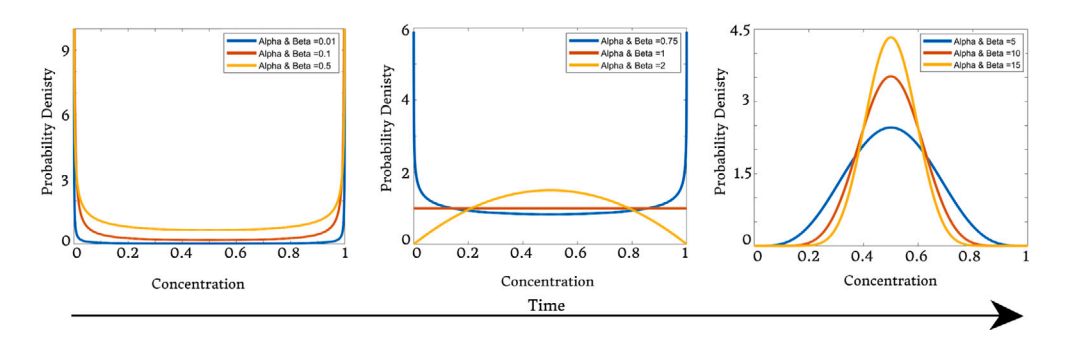


Fig. 6. Illustration of the temporal evolution of the pore-scale concentrations distribution at the mixing interface using beta pdf.

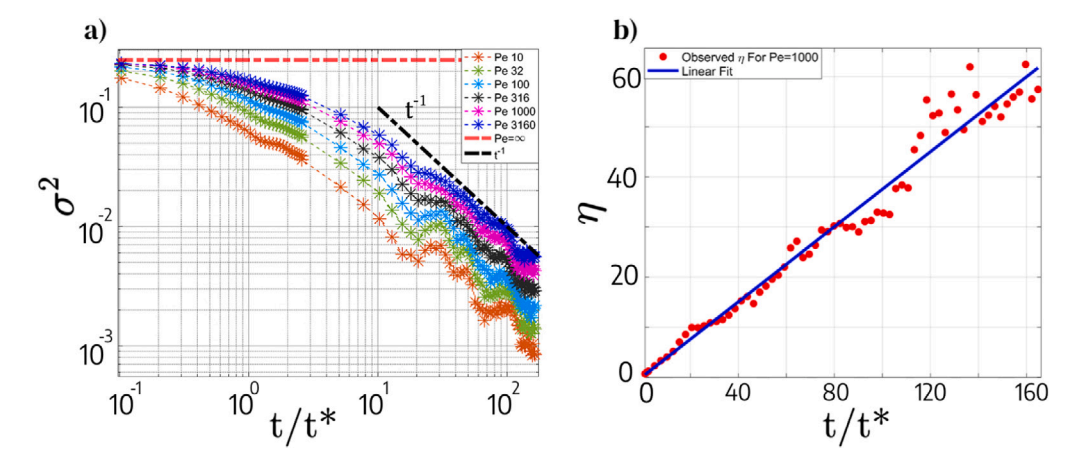


Fig. 7. (a) Variance temporal decay of pore scale concentrations pdfs at  $z_{iif}(t;x,y)|_{\bar{\epsilon}=0.5}$  (b)  $\eta$  linear scaling with time for Pe=1000.

At  $z_{iif}(t;x,y)|_{\bar{c}=0.5}$ , we found that  $\eta$  exhibits a linear scaling with time as illustrated in Fig. 7(b). Here we present the results for Pe=1000, but this linear time-scaling behavior was observed in all other cases. Thus , we assume an empirical model of  $\eta=mt$ , where the slope m can be expressed in terms of Peclet number as:

$$\eta(t, Pe)|_{\bar{c}=0.5} = \kappa P e^{\lambda} t. \tag{20}$$

By conducting a simultaneous fit for all six Peclet cases to minimize the mean squared error between the observed and empirical variance, we determined that the empirical constants  $\kappa$  and  $\lambda$  are  $\sim 0.2 \pm 0.01$  and  $\sim -0.3 \pm 0.02$ , respectively.

If we examine the scenario where  $\bar{c} = 0.5$  and  $\eta(t = 0) = 0$ , Eq. (19) reduces to the initial variance of 0.25. Note that by combining (19) and (20) the decay in variance scales at late times as  $t^{-1}$ ..

To generalize Eq. (20) for any  $\bar{c} \in [0\,1]$ , we analyzed how  $\eta(t,Pe)$  changes for the pdfs away from the interface (i.e,  $z_{itf}(t;x,y)|_{\bar{c}\neq 0.5}$ ). We define  $\eta^*$  as  $\eta$  for  $\bar{c}\in [0\,1]$  normalized by  $\eta$  for  $\bar{c}=0.5$ . By examining how the curves converged, as demonstrated in Fig. 8(a), we infer that  $\eta^*$  is neither time nor Péclet dependent. That is, an invariant relationship exists for  $\eta$  between its value at the middle of the mixing interface and everywhere else, and this relationship holds at all times and across all Péclet values. Therefore, we assume that the spatial variability of  $\eta^*$  for  $\bar{c}\in [0\,1]$  follows a  $\frac{1}{2\sqrt{\bar{c}(1-\bar{c})}}$  shape which fits the data in Fig. 8(a).

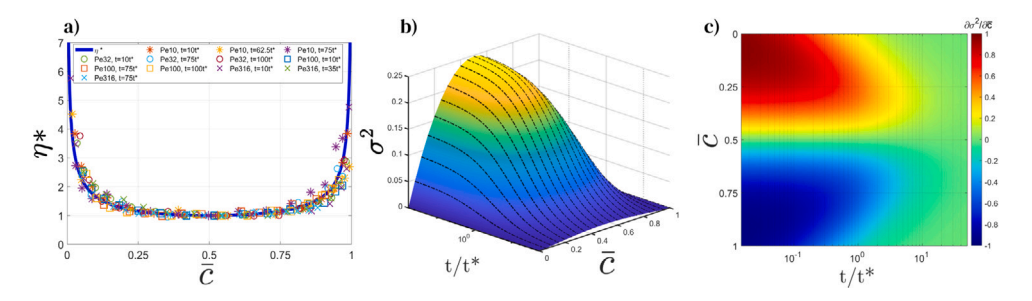


Fig. 8. (a) Observed  $\eta^*$  for different times and Péclet numbers normalized with comparison to  $\eta^* = \frac{1}{2\sqrt{\epsilon(1-\epsilon)}}$  (b) illustration of the pdfs variance as expressed by Eq. (22) at Pe=1000 (c) Heat map for the variance spatial gradient (Eq. (23)) at Pe=1000 showing the transition into a homogeneous system.

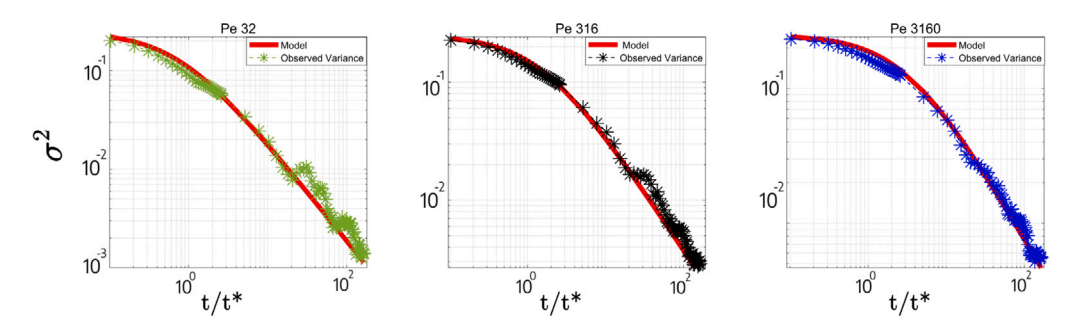


Fig. 9. Temporal decay of the variance of pore-scale concentration pdf at  $z_{iif}(t;x,y)|_{\bar{c}=0.5}$  with comparisons to Eq. (22) for different Péclet cases.

Consequently, we can reformulate Eq. (20) as:

$$\eta(\bar{c}, t, Pe) = \frac{\kappa P e^{\lambda} t}{2\sqrt{\bar{c}(1-\bar{c})}}.$$
 (21)

In this expression the numerator characterizes the temporal evolution of  $\eta$  at the interface  $z_{iif}(t;x,y)|_{\bar{c}=0.5}$  and the denominator quantifies the spatial variation of  $\eta$  across the range of  $\bar{c}$  values from 0 to 1. Thus, Eqs. (17), (18), and (21) provide the full temporal and spatial evolution of the pore-scale concentration pdf under incomplete mixing. Furthermore, we can generalize the expression for the variance by substituting (21) into (19) as:

$$\sigma^{2} = \frac{2\bar{c}^{3/2}(1-\bar{c})^{3/2}}{\kappa P e^{\lambda} t + 2\sqrt{\bar{c}(1-\bar{c})}}.$$
 (22)

Eq. (22) is visually illustrated in Fig. 8(b), showcasing the spatio-temporal decay of the variance. This shows that at any given moment, the pdfs representing concentrations at  $z_{itf}(t;x,y)|_{\bar{c}=0.5}$  exhibit maximum variance, whereas  $\sigma^2$  tends to zero at the extreme values of  $\bar{c}$  of 0 or 1, far from the mixing interface. This explains the deviation from the well-mixed solution being maximum at the mixing interface as previously illustrated in Fig. 4(c).

We can use Eq. (22) to quantify the rate of variance change along the plume (i.e.  $\bar{c} \in [01]$ ). Taking the derivative of Eq. (22) with respect to  $\bar{c}$  we get

$$\frac{\partial \sigma^2}{\partial \bar{c}} = -\frac{(2\bar{c} - 1)\left(3kPe^{\lambda}t\sqrt{(1 - \bar{c})\bar{c}} - 4\bar{c}^2 + 4\bar{c}\right)}{\left(2\sqrt{(1 - \bar{c})\bar{c}} + kPe^{\lambda}t\right)^2} \,. \tag{23}$$

This is illustrated in Fig. 8(c). It shows that after approximately 10 advection times, the variance of pore-scale concentrations fluctuations around their respective mean  $\bar{c}$  becomes approximately uniform along the column. This is not to be confused with being well-mixed which refers to having a constant concentration.

Lastly, to validate Eq. (22), we compare it to the observed variance as presented in Fig. 9. Our model captures the initial rapid decay in the observed variance and subsequently scales as  $t^{-1}$  in a manner consistent with the data.

### 6. Summary and conclusion

In this research, we utilized high-resolution pore-scale simulations, designed to replicate a laboratory scale column experiment, to examine the temporal and spatial changes in probability density functions (pdfs) of pore-scale concentrations. These simulations numerically modeled flow and transport, exploring various Péclet numbers with a focus on scenarios dominated by advection. Our objective was to analyze the pdfs within the context of uniform Darcy-scale flow. However, we recognized that it is crucial to account for unavoidable and ubiquitous boundary effects that persist in confined simulations, despite efforts to mitigate their influence. To address this, we developed a semi-analytical approach to estimate the mean effective transport velocity profile of the mixing interface in the presence of a non-uniform Darcy velocity.

We applied this semi-analytical approach to determine the transverse dispersion coefficient and our measurements closely matched previously published experimental data. While column experiments frequently yield measurements of longitudinal dispersion, transverse dispersion is usually not measured in such settings. Yet, we achieved this through our framework, and we envision the possibility of applying it to experimental setups under specific conditions. This proposed method, with further refinement, has the potential to serve as a valuable tool in obtaining as much information as possible from experiments, taking advantage of unavoidable and typically undesirable boundary effects.

Next, we used this semi-analytical solution to examine the probability density functions (pdfs) capable of describing spatio-temporal changes in pore-scale concentrations. As in many previous studies, in contrast to the common assumption of uniformity at the Darcy scale, our observations revealed that concentrations at the pore-scale mixing interface exhibit non-uniformity. This phenomenon, often referred to as "incomplete mixing", arises from the complex flow dynamics within porous media. In this paper, we demonstrated that among various commonly employed pdfs, the beta pdf is the most consistent and suitable for capturing the complete spatial and temporal evolution of pore-scale concentrations for any  $\bar{c} \in [0,1]$ . Additionally, it was observed that the Truncated Normal distribution becomes a reasonable estimate at asymptotic times, but only at the mixing interface (i.e.,  $\bar{c} = 0.5$ ).

In an effort to upscale, we introduced a model that describes the spatial and temporal decay of the variance of the beta probability density function (pdf). The temporal evolution of the shape parameter  $(\eta)$  at the mixing interface exhibited a linear relationship with time  $t^1$ , but leaves open the question as to what pore-scale mechanisms might explain this scaling. The variance decay model matches observation from the pore-scale simulations of Sole-Mari et al. (2022). Unlike previous approaches, we not only hypothesized but also demonstrated that pore-scale concentrations can be represented by a beta pdf, and that the variance decay can be quantified using the Péclet number and the 1-D Darcy-scale mean concentrations  $(\bar{c})$ . This work was conducted using randomly arranged mono-dispersed granular porous media, encouraging research on its applicability (or lack thereof) in other settings.

#### **Funding**

SF and DB acknowledge funding for this project from the US National Science Foundation via grants EAR-1951677 and EAR-2049688.

#### CRediT authorship contribution statement

Saif Farhat: Writing – original draft, Visualization, Validation, Software, Methodology, Investigation, Formal analysis, Data curation, Conceptualization. Guillem Sole-Mari: Writing – review & editing, Supervision, Software, Resources, Investigation, Conceptualization. Daniel Hallack: Writing – review & editing, Software, Conceptualization. Diogo Bolster: Writing – review & editing, Supervision, Resources, Project administration, Funding acquisition, Conceptualization.

# Declaration of competing interest

The authors declare that they have no known competing financial interests or personal relationships that could have appeared to influence the work reported in this paper.

# Data availability

The processed pore-scale data analyzed within this paper, as well as the maximum likelihood estimation analysis and the semi-analytical approach implementation are available on Zenodo ( <code>https://zenodo.org/records/10442631</code>). The concentration and velocity field data for the entire domain are available upon request, owing to the size limitations of public repositories.

### References

- Acharya, R.C., Valocchi, A.J., Werth, C.J., Willingham, T.W., 2007. Pore-scale simulation of dispersion and reaction along a transverse mixing zone in two-dimensional porous media. Water Resour. Res. 43 (10).
- Alhashmi, Z., Blunt, M., Bijeljic, B., 2015. Predictions of dynamic changes in reaction rates as a consequence of incomplete mixing using pore scale reactive transport modeling on images of porous media. J. Contaminant Hydrol. 179, 171–181.
- Anna, P.d., Jimenez-Martinez, J., Tabuteau, H., Turuban, R., Le Borgne, T., Derrien, M., Méheust, Y., 2014. Mixing and reaction kinetics in porous media: An experimental pore scale quantification. Environ. Sci. Technol. 48 (1), 508–516.
- Atmadja, J., Bagtzoglou, A.C., 2001. State of the art report on mathematical methods for groundwater pollution source identification. Environ. Forensics 2 (3), 205–214.Bazarin, R.L., De Lai, F.C., Naaktgeboren, C., Junqueira, S.L., 2021. Boundary effects on
- Bazarin, R.L., De Lai, F.C., Naaktgeboren, C., Junqueira, S.L., 2021. Boundary effects on the tortuosity and permeability of idealized porous media. Transp. Porous Media 136 (3), 743–764.

- Bellin, A., Severino, G., Fiori, A., 2011. On the local concentration probability density function of solutes reacting upon mixing. Water Resour. Res. 47 (1).
- Bellin, A., Tonina, D., 2007. Probability density function of non-reactive solute concentration in heterogeneous porous formations. J. Contaminant Hydrol. 94 (1-2), 109-125.
- Bijeljic, B., Raeini, A., Mostaghimi, P., Blunt, M.J., 2013. Predictions of non-Fickian solute transport in different classes of porous media using direct simulation on pore-scale images. Phys. Rev. E 87 (1), 013011.
- Bolster, D., Valdés-Parada, F.J., LeBorgne, T., Dentz, M., Carrera, J., 2011. Mixing in confined stratified aquifers. J. Contaminant Hydrol. 120, 198–212.
- Chiogna, G., Bellin, A., 2013. Analytical solution for reactive solute transport considering incomplete mixing within a reference elementary volume. Water Resour. Res. 49 (5), 2589–2600.
- Cirpka, O., Kitanidis, P., 2001. Theoretical basis for the measurement of local transverse dispersion in isotropic porous media. Water Resour. Res. 37 (2), 243–252.
- Delgado, J., 2007. Longitudinal and transverse dispersion in porous media. Chem. Eng. Res. Des. 85 (9), 1245–1252.
- Dentz, M., Tartakovsky, D.M., 2010. Probability density functions for passive scalars dispersed in random velocity fields. Geophys. Res. Lett. 37 (24).
- Elderton, W.P., 1906. Frequency-curves and Correlation. Institute of Actuaries.
- Gramling, C.M., Harvey, C.F., Meigs, L.C., 2002. Reactive transport in porous media: A comparison of model prediction with laboratory visualization. Environ. Sci. Technol. 36 (11), 2508–2514.
- Kapoor, V., Gelhar, L.W., Miralles-Wilhelm, F., 1997. Bimolecular second-order reactions in spatially varying flows: Segregation induced scale-dependent transformation rates. Water Resour. Res. 33 (4), 527–536.
- Le Borgne, T., Dentz, M., Villermaux, E., 2015. The lamellar description of mixing in porous media. J. Fluid Mech. 770, 458–498.
- Liu, M., Mostaghimi, P., 2018. Numerical simulation of fluid-fluid-solid reactions in porous media. Int. J. Heat Mass Transfer 120. 194–201.
- Liu, J., Wilson, J., 1995. Modeling travel time and source location probabilities in twodimensional heterogeneous aquifer. In: Proc. 5th WERC Technology Development Conference. pp. 59–76.
- Oates, P., Harvey, C., 2007. Upscaling reactive transport in porous media: Laboratory visualizations and stochastic models. In: AGU Fall Meeting Abstracts, vol. 2007, pp. H32D-08.
- Ogata, A., Banks, R.B., 1961. A Solution of the Differential Equation of Longitudinal Dispersion in Porous Media. US Government Printing Office.
- Oya, S., Valocchi, A.J., 1998. Transport and biodegradation of solutes in stratified aquifers under enhanced in situ bioremediation conditions. Water Resour. Res. 34 (12), 3323-3334.
- Perez, L.J., Hidalgo, J.J., Dentz, M., 2019. Upscaling of mixing-limited bimolecular chemical reactions in poiseuille flow. Water Resour. Res. 55 (1), 249–269.
- Polyanin, A.D., 2001. Handbook of Linear Partial Differential Equations for Engineers and Scientists. Chapman and Hall/CRC.
- Raje, D.S., Kapoor, V., 2000. Experimental study of bimolecular reaction kinetics in porous media. Environ. Sci. Technol. 34 (7), 1234–1239.
- Rolle, M., Chiogna, G., Hochstetler, D.L., Kitanidis, P.K., 2013. On the importance of diffusion and compound-specific mixing for groundwater transport: An investigation from pore to field scale. J. Contaminant Hydrol. 153, 51–68.
- Rubio, A., Zalts, A., El Hasi, C., 2008. Numerical solution of the advection-reaction-diffusion equation at different scales. Environ. Model. Softw. 23 (1), 90–95.
- Sole-Mari, G., Bolster, D., Fernandez-Garcia, D., 2022. A closer look: High-resolution pore-scale simulations of solute transport and mixing through porous media columns. Transp. Porous Media 1–27.
- Sole-Mari, G., Fernàndez-Garcia, D., Sanchez-Vila, X., Bolster, D., 2020. Lagrangian modeling of mixing-limited reactive transport in porous media: Multirate interaction by exchange with the mean. Water Resour. Res. 56 (8), e2019WR026993.
- Szymczak, P., Ladd, A.J.C., 2003. Boundary conditions for stochastic solutions of the convection-diffusion equation. Phys. Rev. E 68, 036704. http://dx.doi.org/10.1103/ PhysRevE.68.036704, URL https://link.aps.org/doi/10.1103/PhysRevE.68.036704.
- Tartakovsky, A.M., Tartakovsky, G.D., Scheibe, T.D., 2009. Effects of incomplete mixing on multicomponent reactive transport. Adv. Water Resour. 32 (11), 1674–1679.
- Valocchi, A.J., Bolster, D., Werth, C.J., 2019. Mixing-limited reactions in porous media. Transp. Porous Media 130. 157–182.
- Wilson, J., Liu, J., 1994. Backward tracking to find the source of pollution. Water Manage. Risk Remed. 1, 181–199.